Relativistic distorted-wave impulse approximation analysis of ^{12}C(e, $e'p$) for $Q^2 < 2$ (GeV/c)^2

James J. Kelly
Department of Physics, University of Maryland, College Park, Maryland 20742, USA
(Received 1 February 2005; published 30 June 2005)

We analyze data for ^{12}C(e, $e'p$) with $Q^2 < 2$ (GeV/c)^2 using the relativistic distorted-wave impulse approximation (RDWIA) based upon Dirac-Hartree wave functions. The $1p$ normalization extracted from data for $Q^2 > 0.6$ (GeV/c)^2 is approximately 0.87, independent of Q^2, which is consistent with the predicted depletion of the $1p_{3/2}$ orbital by short-range correlations. The total $1p$ and $1s$ strength for $E_m < 80$ MeV approaches 100% of IPSM (independent particle shell model), consistent with a continuum contribution for $30 < E_m < 80$ MeV of about 12% of IPSM. Similarly, a scale factor of 1.12 brings RDWIA calculations into good agreement with ^{12}C(e, $e'p$) data for transparency. We also analyzed low Q^2 data from which a recent nonrelativistic RDWIA analysis suggested that spectroscopic factors might depend strongly upon the resolution of the probe. We find that the momentum distributions for their empirical Woods-Saxon wave functions fit to low Q^2 data for parallel kinematics are too narrow to reproduce data for quasiperpendicular kinematics, especially for larger Q^2, and are partly responsible for reducing fitted normalization factors. Although the RDWIA normalization factors for $Q^2 < 0.2$ (GeV/c)^2 are also smaller than obtained for $Q^2 > 0.6$ (GeV/c)^2, the effect is smaller, and we argue that it should be attributed to the effective single-nucleon current operator instead of to spectroscopic factors, which are probe-independent properties of nuclear structure. However, remediation of the failure of RDWIA calculations to reproduce low Q^2 data for parallel kinematics will require a more sophisticated modification of the current method than a simple multiplicative factor.

DOI: 10.1103/PhysRevC.71.064610 PACS number(s): 25.30.Fj, 27.20.+n, 21.10.Jx, 24.10.Jv

I. INTRODUCTION

It is generally believed that single-nucleon electromagnetic knockout provides unambiguous measurements of the momentum distributions and spectroscopic factors for single-hole states near the Fermi surface. Reviews of analyses based upon the nonrelativistic distorted-wave impulse approximation (NRDWIA) can be found in Refs. [1–3], which show that the momentum distributions are described well by mean-field calculations, such as Skyrme-Hartree-Fock, while spectroscopic factors for low-lying states are reduced relative to the independent particle shell model (IPSM) by an average factor of about 65% over a broad range of A. Part of the depletion of IPSM strength can be attributed to short-range correlations that shift approximately 15% of the hole strength to very large missing energies, beyond 100 MeV. Recently, a direct measurement of the spectral function using ^{12}C(e, $e'p$) in parallel kinematics [4] observed approximately 0.6 protons in a region with $p_m \gtrsim 240$ MeV/c and $E_m \gtrsim 50$ MeV attributable to single-nucleon knockout from correlated clusters. This finding is consistent with the 16% IPSM predicted by Frick *et al*. [5] using the self-consistent Green's function (SCGF) method [6]. Similar estimates of the depletion of hole states are also available from the correlated basis function (CBF) theory [7] and other methods. Furthermore, SCGF calculations [8,9] show that the momentum distributions for low-lying quasihole states are hardly affected by short-range correlations, remaining very similar to mean-field calculations, while the momentum distributions for the large-E_m continuum are substantially broadened.

If the occupancy of IPSM orbitals is predicted to be approximately 85% by theories that reproduce the correlated strength at large (E_m, p_m), why is only 65% observed by (e, $e'p$) experiments? Coupling to collective modes is expected to produce significant fragmentation of the valence quasihole strength spread over a range of perhaps 10 MeV, but the extended random-phase-approximation (RPA) calculations presently available do not yet reproduce those fragmentation patterns well [6]. Thus, it is possible that many small fragments are missed experimentally even if they lie within the experimental acceptance. Alternatively, problems in the reaction model may lead to systematic underestimation of spectroscopic factors. Most of the data contributing to the aforementioned estimate of 65% IPSM were limited to $T_p < 100$ MeV and were analyzed using NRDWIA calculations based upon empirical Woods-Saxon wave functions. More recent analyses based on the relativistic distorted-wave approximation (RDWIA) typically produce larger spectroscopic factors [10] and describe interference response functions more accurately [11–13]. The effects due to dynamical enhancement of Dirac spinors by the nuclear mean field are actually stronger at low Q^2 than at higher energies [14].

While spectroscopic factors are of obvious importance to theories of nuclear structure, they also affect analyses of nuclear transparency that look for the onset of color transparency [15,16]. Those experiments typically compare the (e, $e'p$) yield integrated over wide but finite ranges of missing momentum p_m and missing energy E_m with calculations based upon a model spectral function. This spectral function is usually based upon the IPSM with a correction factor for the depletion by correlations of the single-hole strength within the experimental acceptance. Therefore, the accuracy of the depletion factor affects the accuracy of transparency measurements.

Recently Lapikás *et al.* [17] analyzed the data for ^{12}C$(e, e'p)$ with $Q^2 < 0.4$ (GeV/c)^2 using NRDWIA calculations with Woods-Saxon bound-state wave functions fit to the NIKHEF data for $T_p = 70$ MeV in parallel kinematics [18] and concluded that the normalization factors relative to IPSM were $N_{1p} = 0.56 \pm 0.02$ and $N_{1s} = 0.59 \pm 0.04$ for $E_m < 80$ MeV. They then argued that the transparency results based upon an estimated depletion factor of $f = 0.9$ for the single-hole spectral function with $E_m < 80$ MeV should be increased by a factor of approximately 1.25 using appropriately weighted attenuation factors for the $1p$ and $1s$ shells. Finally, they argued that the normalization factors for ^{12}C vary strongly with Q^2 from the low values fitted to the NIKHEF data to values approaching the IPSM limit for $Q^2 > 2$ (GeV/c)^2. Frankfurt *et al.* [19] speculated that quenching of spectroscopic factors for low Q^2 might be caused by probing a dressed quasiparticle using long wave lengths and that at higher resolution the effective current operator for the $(e, e'p)$ reaction approaches more closely that for a free nucleon. However, although the Q^2 range was smaller, our recent relativistic analysis showed no significant slope in the normalization factors fit to ^{16}O$(e, e'p)$ data for $Q^2 < 0.8$ (GeV/c)^2 [20]. Furthermore, we find that RDWIA calculations based upon the ordinary single-nucleon current with dynamical enhancement of lower components of Dirac spinors describe the left-right asymmetry for quasiperpendicular kinematics very well [14]; it is not obvious that one should describe quasiparticles for low Q^2 using Dirac spinors in a similar mean field.

In this paper we use RDWIA calculations to analyze the data for ^{12}C$(e, e'p)$ with $Q^2 \lesssim 2$ (GeV/c)^2. In addition to the data considered by Lapikás *et al.* [17], we include recent data from Dutta *et al.* [15] for $Q^2 = 0.6$, 1.2, and 1.8 (GeV/c)^2. Our RDWIA fits produce systematically larger normalization factors using Dirac-Hartree wave functions than using the Woods-Saxon wave functions that were fit to the NIKHEF data. The latter do not describe well the momentum distributions for larger Q^2; nor do they describe the data for low Q^2 with quasiperpendicular kinematics as well as do Dirac-Hartree wave functions. Therefore, the fits to data for parallel kinematics with small ejectile energies appear to produce artificially narrow momentum distributions that result in anomalously low spectroscopic factors.

The model and fitting procedures are described in Secs. II and III. Section IV presents an analysis based upon an approximation that permits direct comparison between nonrelativistic and relativistic bound-state wave functions. Section V presents a more rigorous analysis of both spectroscopic factors and transparency using RDWIA. Our conclusions are summarized in Sec. VI.

II. REACTION MODELS

Detailed descriptions of RDWIA for $(e, e'p)$ reactions have been given in many recent papers. Here we briefly discuss those aspects relevant to the current application and refer to Refs. [14,20] for further details. In RDWIA, a nuclear matrix element of the single-nucleon electromagnetic current for the $A(e, e'N)B$ reaction takes the form

$$\mathcal{J}^\mu = \int d^3r \exp(i\boldsymbol{t}\cdot\boldsymbol{r})\langle\Psi^{(-)}(\boldsymbol{p}', \boldsymbol{r})|\gamma^0\Gamma^\mu(\boldsymbol{p}', \boldsymbol{p}' - \boldsymbol{q})|\Phi(\boldsymbol{r})\rangle, \tag{1}$$

where Γ^μ is the vertex function, $\boldsymbol{q}$ is the momentum transfer, $\boldsymbol{p}'$ is the ejectile momentum, and $\boldsymbol{t} = E_B\boldsymbol{q}/W$ is the recoil-corrected momentum transfer. The overlap Φ between initial and final nuclear states, often called the bound-state wave function, is approximated by a bound solution of a Dirac equation with real scalar and vector potentials. Similarly, the ejectile distorted wave $\Psi^{(-)}$ is an incoming solution to a Dirac equation with complex scalar and vector optical potentials. It is convenient to express this matrix element in the form

$$\mathcal{J}^\mu = \int d^3r \exp(i\boldsymbol{t}\cdot\boldsymbol{r})\langle\psi^{(-)}(\boldsymbol{p}', \boldsymbol{r})|J^\mu|\phi(\boldsymbol{r})\rangle, \tag{2}$$

where

$$J^\mu(\boldsymbol{p}', \boldsymbol{p}) = \tilde{\Omega}_c(\boldsymbol{p}', r)\gamma^0\Gamma^\mu\Omega_b(\boldsymbol{p}, r) \tag{3}$$

is a 2×2 current operator that acts upon solutions of second-order equations

$$\left[\nabla^2 + E_c^2 - m^2 - 2E_c\left(U_c^C + U_c^{\rm LS}\boldsymbol{L}\cdot\boldsymbol{\sigma}\right)\right]\psi = 0, \tag{4a}$$

$$\left[\nabla^2 + E_b^2 - m^2 - 2E_b\left(U_b^C + U_b^{\rm LS}\boldsymbol{L}\cdot\boldsymbol{\sigma}\right)\right]\phi = 0, \tag{4b}$$

which now take the form of Pauli spinors. The subscripts b and c refer to bound and continuum wave functions. These equations feature central and spin-orbit Schrödinger potentials, U^C and $U^{\rm LS}$, obtained from the corresponding scalar and vector Dirac potentials, S and V, using the well-known formulas [21,22]

$$U^C = V + \frac{m}{E}S + \frac{S^2 - V^2}{2E} + U^D, \tag{5a}$$

$$U^D = \frac{1}{2E}\left[-\frac{1}{2r^2D}\frac{d}{dr}(r^2D') + \frac{3}{4}\left(\frac{D'}{D}\right)^2\right], \tag{5b}$$

$$U^{\rm LS} = -\frac{1}{2E}\frac{D'}{rD}, \tag{5c}$$

where V includes the Coulomb potential and where

$$D(r) = 1 + \frac{S(r) - V(r)}{E + M} \tag{6}$$

is known as the Darwin nonlocality factor. Often it is more convenient to express the Darwin factor in terms of the spin-orbit potential using [23]

$$D(r) = \exp\left[2E\int_r^\infty dr' r'\, U^{\rm LS}(r')\right]. \tag{7}$$

The spinor-distortion operators are given by

$$\Omega_\alpha(\boldsymbol{p}, r) = \begin{pmatrix} 1 \\ \dfrac{\sigma\cdot p}{(E+m)D_\alpha(r)} \end{pmatrix} D_\alpha^{1/2}(r), \tag{8}$$

where $\alpha \in \{b, c\}$ and where the lower component uses the momentum operator and the appropriate Darwin factor. These representations of the RDWIA matrix element are completely

equivalent, but the 2×2 representation facilitates approximations that are useful for comparing RDWIA and NRDWIA calculations.

To understand the small spectroscopic factors obtained by Lapikás *et al.* [17], it will be useful to present RDWIA calculations based upon their Woods-Saxon wave functions. For this purpose, we replace their Perey nonlocality factor by a Darwin factor computed using Eq. (7) with the Woods-Saxon spin-orbit potential. Such potentials are usually expressed in the form

$$U^{\rm LS}(r) = \frac{2}{r}\frac{\partial}{\partial r}\frac{V_{\rm LS}}{1+\exp[(r-R_{\rm LS})/a_{\rm LS}]}, \tag{9}$$

where $V_{\rm LS}$, $R_{\rm LS}$, and $a_{\rm LS}$ are strength, radius, and diffuseness parameters and where $V_{\rm LS} > 0$. The corresponding Darwin factor then takes the form

$$D(r) = \exp\left(-\frac{4mV_{\rm LS}}{1+\exp[(r-R_{\rm LS})/a_{\rm LS}]}\right) \tag{10}$$

and is used in Eq. (8) to produce the lower component needed for RDWIA. However, because this Darwin factor is not the same as the original Perey factor, this prescription alters the momentum distribution.

To better simulate the momentum distribution for NRDWIA calculations with Woods-Saxon wave functions, we will also show EMA-noSV calculations using the Perey factor instead of the Darwin factor. The EMA-noSV approximation to RDWIA was introduced in Refs. [2,11], and its relationship to full RDWIA is explored in more detail in Ref. [14]. The basic idea is that the missing momentum distribution is determined by the upper component of the bound-state wave function, while the lower component is constructed using the relationship for free Dirac spinors, such that

$$\Omega(\boldsymbol{p}, r) \longrightarrow \begin{pmatrix} 1 \\ \dfrac{\sigma \cdot p}{E+m} \end{pmatrix} D^{1/2}(r), \tag{11}$$

where the momentum for the lower component is based upon asymptotic kinematics. Thus, for the bound state, we use $\boldsymbol{p} = \boldsymbol{p}' - \boldsymbol{q}$ and $E = \sqrt{m^2 + p^2}$. This approximation permits use of the relativistic current operator without need of p/m expansions to obtain a nonrelativistic limit and produces a momentum distribution that is very similar to that for a full RDWIA calculation, but it does not reproduce the left-right asymmetry as well because it neglects the distortion of the lower component by the mean field [11,14]. Also note that the Darwin factor is retained because it affects the momentum distribution and is computed according to Eq. (7) for Dirac-Hartree wave functions. When using Woods-Saxon wave functions, on the other hand, we replace the Darwin factor for EMA-noSV with the customary Perey nonlocality factor [24], such that

$$\Omega_b(\boldsymbol{p}, r) \longrightarrow \begin{pmatrix} 1 \\ \dfrac{\sigma \cdot p}{E+m} \end{pmatrix} P_b^{1/2}(r), \tag{12}$$

where

$$P_b(r) = \left[1 - \frac{m\beta_{\rm NL}^2}{2}U_b^C(r)\right]^{-1} \tag{13}$$

is based upon the central binding potential and where $\beta_{\rm NL} \sim 0.85$ fm. The reduced cross section is then practically identical to the missing momentum distribution for the corresponding traditional NRDWIA calculation using the same potentials and nonlocality factors. Therefore, the EMA-noSV analysis using various Dirac-Hartree or Woods-Saxon wave functions evaluates the effects of differences in the momentum distribution, whereas the full RDWIA analysis with Dirac-Hartree wave functions is more accurate because it also includes the effects of distortion of lower components of Dirac spinors.

It is important to recognize that even though the Darwin factor in Eq. (10) is similar to the Perey factor in Eq. (13), they are not identical because nonrelativistic spin-orbit and central potentials are adjusted independently and are not derived from scalar and vector potentials in the same manner as for relativistic calculations. This difference alters the momentum distribution. For the particular case considered here, the replacement $P \rightarrow D$ produces a somewhat narrower momentum distribution for RDWIA than for EMA-noSV using the same Woods-Saxon wave function; this difference reduces the spectroscopic factor fitted to data.

Finally, all calculations treat electron distortion in the $q_{\rm eff}$ approximation [25] and use the CC2 current operator [26]

$$\Gamma^\mu = \gamma^\mu F_1(Q^2) + i\sigma^{\mu\nu}\frac{\bar{q}_\nu}{2m}F_2(Q^2), \tag{14}$$

with MMD form factors [27] in Coulomb gauge. The momentum transfer is evaluated on-shell, such that $\bar{q} = (E' - E, \boldsymbol{p}' - \boldsymbol{p})$ with $\boldsymbol{p} = \boldsymbol{p}' - \boldsymbol{q}_{\rm eff}$ where $\boldsymbol{q}_{\rm eff}$ is the effective momentum transfer, $\boldsymbol{p}'$ is the ejectile asymptotic momentum, and the energies E and E' are on shell; the form factors use $Q^2 = \boldsymbol{q}^2 - \omega^2$ where $(\omega, \boldsymbol{q})$ are based upon the electron-scattering kinematics. Optical potentials for the ejectile were taken from the global analysis by Cooper *et al.* [28]. We consider Dirac-Hartree wave functions from the original Horowitz and Serot analysis (HS) [29] and the nonlinear analysis from Sharma *et al.* (NSLH) [30]. In addition, we consider the Woods-Saxon wave functions used by Lapikás *et al.* [17] in their NRDWIA analysis of ^{12}C$(e, e'p)$.

III. DATA AND FITTING PROCEDURES

The data we consider are summarized in Table I. Reduced cross sections for the Tokyo, Saclay, and SLAC data were provided by Lapikás [17,31] and include small adjustments to a common convention for reduced cross section. In addition, radiative corrections were applied to the data from Ref. [32]. Only for the NIKHEF experiment [18] was it possible to resolve the lowest three $1p$ fragments. Although there are small differences between the missing momentum distributions for these three fragments, the ground state represents about 81% and the next $1p_{3/2}$ fragment an additional 9% of the total $1p$ strength for $E_m < 25$ MeV. Therefore, we represent the $1p$ strength using either a single Dirac-Hartree wave function for

TABLE I. Summary of data for $^{12}C(e, e'p)$. E_0 is the beam energy and T_p is the central proton kinetic energy. Quasiperpendicular kinematics with constant $(\omega, \boldsymbol{q})$ were used unless a Q^2 range is given.

Data set	E_0 (MeV)	$\Delta E_m(1p)$ (MeV)	$\Delta E_m(1s)$ (MeV)	T_p (MeV)	Q^2 [(GeV/c)^2]	Notes
Tokyo [34]	700	6–30	21–66	159	0.29	
	700		21–66	136		
Saclay [35]	497	15–22	30–50	87	0.16	
Saclay [32]	500	15–22	NA	99	0.18	Constant $(\omega, \boldsymbol{q})$
Saclay [32]	500	15–22	NA	99	0.09–0.32	Parallel; 1s not available
NIKHEF[a] [18]	285–481	15–22	30–39	70	0.02–0.26	Parallel
SLAC[b] [36]	2015	15–25	30–80	600	1.11	1s not radiatively unfolded
JLab[c] [15]	2445	15–25	30–50	350	0.64	Inclusive bin with $10 \leqslant E_m \leqslant 80$ MeV available
	2445			700	1.28	
	3245			970	1.84	

[a]Nationaal Instituut voor Kernfysica en Hoge-Energiefysica, Netherlands.
[b]Stanford Linear Accelerator Center.
[c]Jefferson Laboratory (JLab) = Thomas Jefferson National Accelerator Facility.

$1p_{3/2}$ or the NIKHEF fit to the ground state. That experiment was also able to resolve several weak positive-parity states with $E_m < 30$ MeV, but their strength is small enough to neglect in the present analysis [33]. For most other experiments, the lowest missing energy bin contains a small contribution from the low-energy tail of the 1s shell. Furthermore, for all experiments the bin intended to emphasize the 1s shell inevitably contains contributions from a broad continuum that may include additional $1p$ strength. Therefore, each E_m bin will be fit as an incoherent mixture of $1p$ and 1s contributions according to

$$\sigma_{\rm red} = N_{1p}\sigma_{\rm red}(1p_{3/2}) + N_{1s}\sigma_{\rm red}(1s_{1/2}), \qquad (15)$$

where the overlap function for each shell is assumed to be independent of missing energy and is normalized to full occupancy. In addition, for the JLab data sets, we fit a normalization factor for the independent particle shell model (IPSM) to the inclusive data in the range $10 \leqslant E_m \leqslant 80$ MeV according to

$$\sigma_{\rm red} = N_{\rm IPSM}[\sigma_{\rm red}(1p) + \sigma_{\rm red}(1s)]. \qquad (16)$$

Calculations will be shown for the entire p_m range measured for each data set, but only data in the range $|p_m| \leqslant 200$ MeV/c will be used to fit the normalization factors because larger p_m may be susceptible to increasing corrections for effects not contained in the RDWIA model based upon single-nucleon current operators (such as short-range correlations, two-body currents, or channel coupling in final-state interactions).

We also require a model of the 1s energy distribution to obtain the spectroscopic factor from the normalization $N_{1s}(E_{\rm min}, E_{\rm max})$ fitted to limited and variable intervals of E_m. One often employs a Lorentzian distribution

$$L_{1s}(E_m) = \frac{1}{2\pi}\frac{\Gamma(E_m)}{(E_m - E_{1s})^2 + [\Gamma(E_m)/2]^2}, \qquad (17)$$

whose energy-dependent width is given by the Brown-Rho parametrization [37]

$$\Gamma(E_m) = \frac{a(E_m - E_F)^2}{(E_m - E_F)^2 + b}, \qquad (18)$$

where E_F is the Fermi energy and a, b are constants. For now, it suffices to use the parameters $a = 24$ MeV and $b = 500$ MeV^2 originally proposed by Brown and Rho [37] with $E_F = 15.96$ MeV and $E_{1s} = 39$ MeV for ^{12}C. Lapikás *et al*. obtained slightly different parameters for b and E_{1s} by fitting the Tokyo data, but the effect upon S_{1s} was insignificant. Thus, one would expect approximately 11% of the 1s strength to be broadly distributed above the 80 MeV missing energy, which is consistent with the depletion factor attributed to short-range correlations. Therefore, in the absence of background, the 1s spectroscopic factor deduced from a fitted normalization factor would be

$$S_{1s} = 2N_{1s}(E_{\rm min}, E_{\rm max})\frac{\int_0^\infty L_{1s}(E_m)dE_m}{\int_{E_{\rm min}}^{E_{\rm max}} L_{1s}(E_m)dE_m}. \qquad (19)$$

IV. EMA-noSV ANALYSIS

Figure 1 compares momentum distributions for the relativistic HS and NLSH models with the Woods-Saxon models used by Lapikás *et al*. [17] and by Dutta *et al*. [15]. The latter were based upon a NRDWIA analysis of the Saclay data for $T_p = 99$ MeV made by Bernheim *et al*. [32]. The differences between the HS and NLSH wave functions are relatively small, but the NIKHEF $1p$ wave function has a much stronger peak and declines more rapidly with respect to p_m. Similarly, the NIKHEF 1s wave function starts higher and falls faster than the relativistic wave functions. Interestingly, the Saclay wave functions show similar behavior, but the effects, compared with the NIKHEF wave functions, are smaller for the $1p$ and larger for the 1s wave function. The large spread among these momentum distributions will obviously be reflected in the corresponding DWIA calculations.

To evaluate the effect of variations of $\rho(p_m)$ upon DWIA calculations using both relativistic and nonrelativistic wave functions, it is simplest to employ the EMA-noSV approach [11]. Several previous papers have shown that the differences between EMA-noSV and full RDWIA calculations

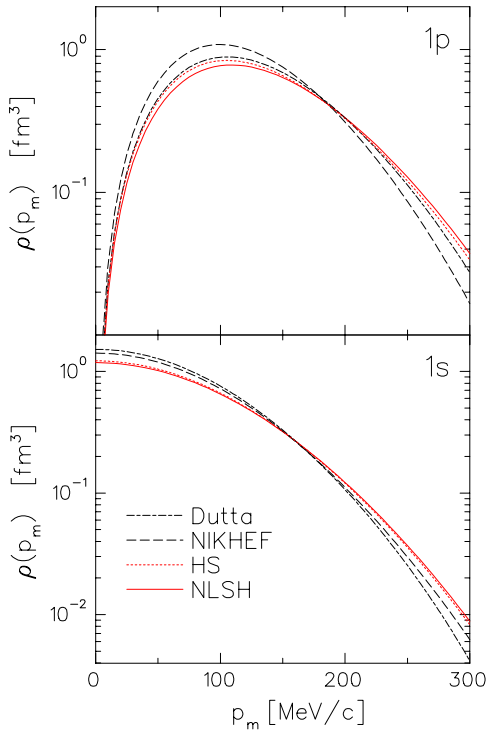

FIG. 1. (Color online) Momentum distribution for ^{12}C$(e, e'p)$.

are relatively small for cross sections [20,38]. Although that approximation does not provide the best description of the left-right asymmetry A_{LT}, it has the advantage that the nonrelativistic wave function can be used directly [11,14]. We use Eqs. (11) and (7) for NLSH and HS wave functions or Eqs. (12) and (13) for NIKHEF wave functions.

Figure 2 compares EMA-noSV calculations using NLSH, HS, and NIKHEF wave functions with the JLab data for $Q^2 = 0.6$, 1.2, and 1.8 $(\mathrm{GeV}/c)^2$. For each kinematics, the top set is semi-inclusive data for $E_m < 80$ MeV, the second set shows a bin $15 \leqslant E_m \leqslant 25$ MeV dominated by the $1p$ shell, and the bottom set shows a bin $30 \leqslant E_m \leqslant 50$ MeV dominated by the $1s$ shell. The curves were fitted to data in the range $|p_m| \leqslant 200$ MeV/c neglecting, at present, the mixing between the shells. We will later find that filling of the $1p$ minimum and broadening of the $1s$ distribution can be described by mixing. These calculations employ the EDAD1 optical potential [28]; other choices of potentials from Cooper *et al.* [28] produce small variations in the normalization factors with little dependence upon the choice of overlap function and practically no discernible effect upon the curves. The results for the two relativistic wave functions, NLSH and HS, are very similar but the fitted p_m distributions for the NIKHEF wave function tend to be too narrow, especially for the $1p$ shell. Consequently, the $1p$ normalization factors listed in Table II are systematically smaller for the NIKHEF wave function than for the NLSH or HS wave functions. These normalization factors are correlated well with the peak of the momentum distribution, with the NLSH results largest, NIKHEF results smallest, and HS in between.

Similar comparisons are shown in Figs. 3–5 for several low Q^2 experiments performed using quasiperpendicular kinematics. Except when noted otherwise, a normalization factor for each curve was obtained using a least-squares fit to the data for $|p_m| \leqslant 200$ MeV/c. Figure 3 shows that the relativistic wave functions describe the data for the Saclay experiment with $T_p = 87$ MeV in quasiperpendicular kinematics better than the NIKHEF wave functions, which fall too rapidly with increasing p_m. The results shown in Fig. 5 for the Tokyo experiment with $Q^2 = 0.29$ $(\mathrm{GeV}/c)^2$

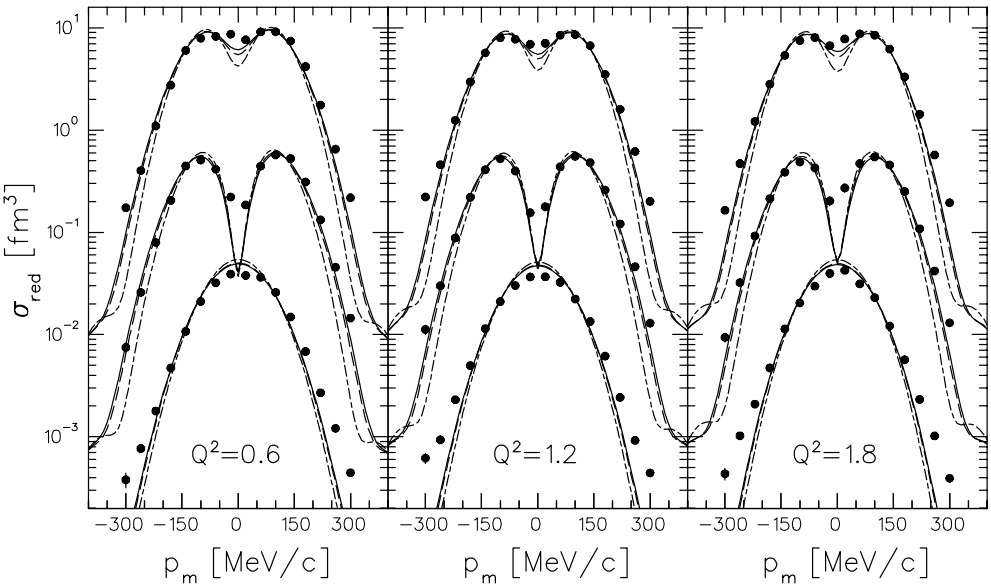

FIG. 2. EMA-noSV calculations for ^{12}C$(e, e'p)$ are compared with quasiperpendicular data for $0.6 < Q^2 < 1.8$ $(\mathrm{GeV}/c)^2$ from JLab [15]. In each panel, the top set of curves shows the inclusive $10 \leqslant E_m \leqslant 80$ MeV bin scaled by a factor of 20; the middle set, the p-shell bin with $15 \leqslant E_m \leqslant 25$ MeV; and the bottom set, the s-shell bin with $30 \leqslant E_m \leqslant 50$ MeV scaled by a factor of 0.1. Solid, dashed, and dash-dotted curves are based upon NLSH, HS, and NIKHEF wave functions, respectively.

TABLE II. Normalization factors for ^{12}C$(e, e'p)(1p)^{-1}$ fitted to quasiperpendicular data for the $1p$ bin using several overlap functions in the EMA-noSV approximation. Possible $1s$ contributions were neglected. The first set uses the EDAD1 and the second the EDAIC optical potential [28].

Experiment	Q^2	E_m	EDAD1			EDAIC		
	[(GeV/c)^2]	(MeV)	NLSH	HS	NIKHEF	NLSH	HS	NIKHEF
Saclay	0.16	15–22	0.637	0.599	0.483	0.572	0.542	0.444
Saclay	0.18	15–22	0.757	0.705	0.554	0.684	0.640	0.510
JLab	0.6	15–25	0.934	0.878	0.697	0.909	0.856	0.682
SLAC	1.1	15–25	0.852	0.791	0.613	0.887	0.822	0.633
JLab	1.2	15–25	0.904	0.849	0.671	0.950	0.890	0.699
JLab	1.8	15–25	0.901	0.854	0.689	0.886	0.841	0.679

are somewhat ambiguous: although the NLSH and HS wave functions give better fits for $p_m \gtrsim 60$ MeV/c, particularly for the ground state, none of the calculations can describe the enhancement at lower p_m seen for the ground state or the dip for the s state. The low p_m bulge for the ground-state data seems somewhat implausible, and there likely were difficulties in cleanly separating the $1p$ and $1s$ contributions to the low p_m data. Therefore, the $1p$ normalization for this set was fitted to $50 \leqslant p_m \leqslant 200$ MeV/c. Similar calculations are also compared with the SLAC data for $Q^2 = 1.1$ (GeV/c)^2 in Fig. 6. We again find that the p_m distribution for the NIKHEF wave function is too narrow to fit the $1p$ data well. However, the $1s$ data remain well above all of the calculations for large p_m. Lapikás *et al*. [17] attributed this problem to $1p$ contamination due to inadequate radiative unfolding.

The normalization factors obtained for single-component EMA-noSV fits are listed in Table II; improved two-component RDWIA fits will be presented in the next section.

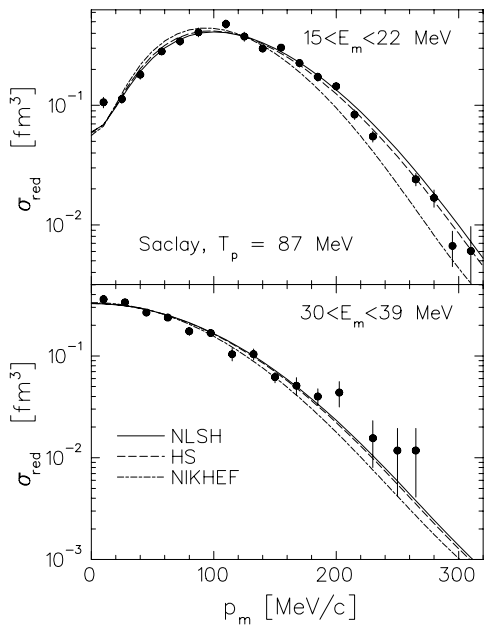

FIG. 3. EMA-noSV calculations for ^{12}C$(e, e'p)$ are compared with quasiperpendicular data for $T_p = 87$ MeV from Saclay [35]. Solid, dashed, and dash-dotted curves are based upon NLSH, HS, and NIKHEF wave functions, respectively.

The Tokyo result is omitted because the $1s$ admixture is appreciable. We find that these factors are correlated well with the peak value of the $\rho(p_m)$, such that the NIKHEF wave functions produce the smallest and the NLSH wave functions the largest normalization factors. Over a wide range of Q^2, including both early data at low Q^2 and recent data for $Q^2 \sim 1$ (GeV/c)^2, the relativistic wave functions fit the p_m distributions relatively well, while the NIKHEF wave functions are systematically narrower than the data. Thus, the data for quasiperpendicular kinematics consistently prefer the broader p_m distributions and larger normalization factors obtained with Dirac-Hartree wave functions.

The data for parallel kinematics, on the other hand, present special problems. We omit the Mainz data [39] because there appear to be significant normalization problems for that experiment [17]. The NIKHEF and Saclay data for parallel kinematics are compared with EMA-noSV calculations for NLSH, HS, and NIKHEF wave functions in Figs. 7 and 8. The results for both experiments are similar but none of these calculations reproduce the data for the $1p$ shell. Because of obvious difficulties for $p_m < 0$, the normalization factors listed in Table III were fitted to $0 < p_m < 200$ MeV/c. These factors are also correlated with the peak values of $\rho(p_m)$ but these fits underestimate the cross sections for $p_m < 0$ and larger Q^2.

To improve standard NRDWIA calculations for parallel kinematics, van der Steenhoven *et al*. [18,40] resorted to adjusting simultaneously the overlap function, the optical model, and the current operator. The NIKHEF analysis used the nonrelativistic expansion of the current operator in powers

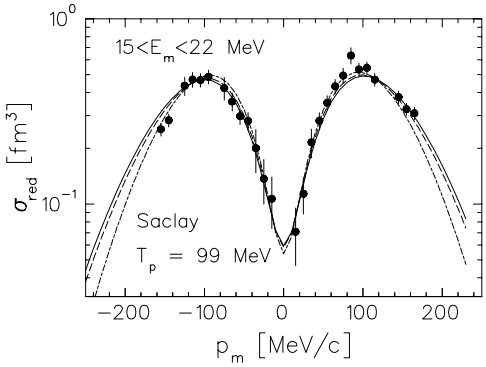

FIG. 4. Same as Fig. 3, but for $T_p = 99$ MeV from Saclay [35].

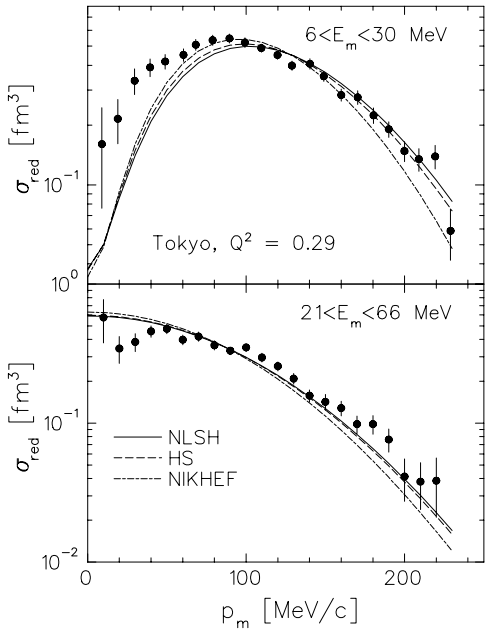

FIG. 5. Same as Fig. 3, but for $Q^2 = 0.29$ (GeV/c)^2 from Tokyo [34].

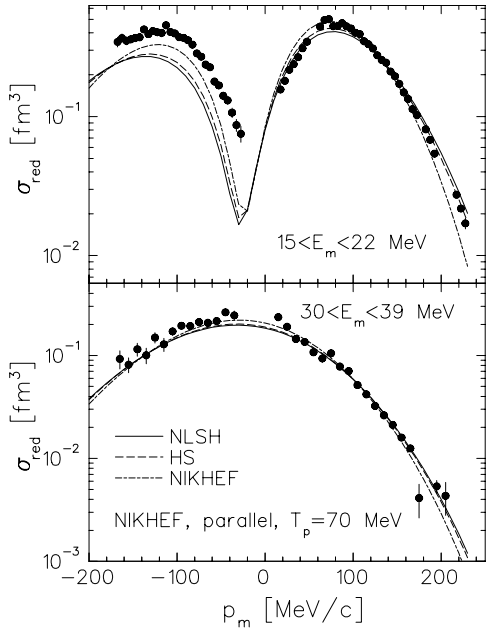

FIG. 7. EMA-noSV calculations for ^{12}C$(e, e'p)$ are compared with data from NIKHEF [18] using parallel kinematics for $T_p =$ 70 MeV/c.

of p/m proposed by McVoy and van Hove [41]; we verified that at second order this expansion, denoted NR2, gives results that are practically indistinguishable from our EMA-noSV calculations. Their analysis also used a nonrelativistic optical potential produced by Comfort and Karp [42], denoted CK, and a Perey factor [24] for the ejectile with $\beta = 0.85$ fm. Figure 9 compares several variations of the NR2 calculations that are similar to those of van der Steenhoven *et al*. The dashed curve uses this optical potential and current operator with the upper component of the NLSH wave function and fails to reproduce the data for parallel kinematics with $p_m < 0$; the results are similar to those shown in Fig. 7 in the EMA-noSV approach. The narrower NIKHEF momentum distribution improves the fit to the data but appears to be shifted to the left—a shift to the right was accomplished by modifying the optical potential. This modified potential, denoted MCO in Ref. [18], was intended to simulate channel coupling in the final state but our more detailed analysis of channel coupling [43] gave much smaller effects for this reaction; hence, we regard this modification of the optical potential to be somewhat *ad hoc*. Finally, van der Steenhoven *et al*. inserted an enhancement factor for transverse components of the current operator and adjusted that factor to fit the peak for negative p_m. Applying this factor without further adjustment does provide a reasonably accurate fit to the reduced cross section for parallel kinematics.

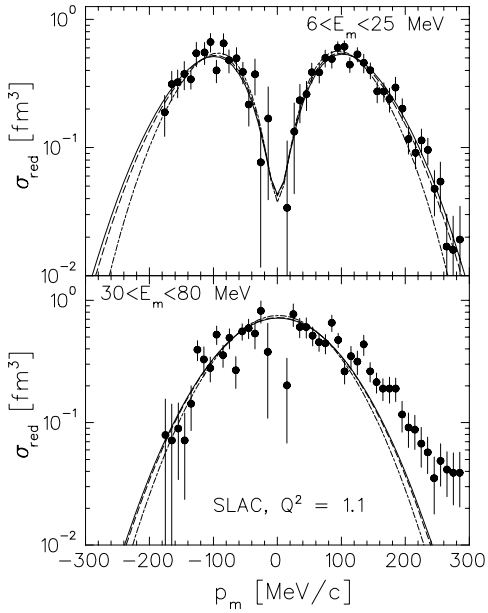

FIG. 6. Same as Fig. 3, but for $Q^2 = 1.1$ (GeV/c)^2 from SLAC [36].

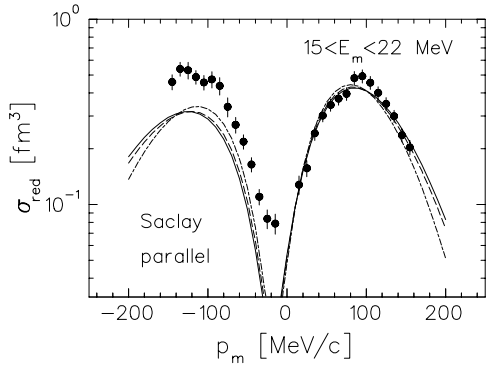

FIG. 8. Same as Fig. 7, but for data from Saclay [32] using parallel kinematics for $T_p = 99$ MeV.

TABLE III. Normalization factors for $^{12}C(e,e'p)(1p)^{-1}$ fitted to data for parallel kinematics using several overlap functions in the EMA-noSV approximation. These results were extracted for the $15 \leqslant E_m \leqslant 22$ MeV bin using NLSH wave functions and the EDAD1 optical potential.

Experiment	T_p	NLSH	HS	NIKHEF
NIKHEF	70	0.635	0.616	0.541
Saclay	99	0.685	0.636	0.505

We have not attempted to tune this fit because we doubt that it is really possible to distinguish between variations of the overlap function, the current operator, and the final-state interactions using these data. Nor does it appear possible to fit the low Q^2 data for both parallel and quasiperpendicular kinematics simultaneously using unique overlap functions and global optical potentials fitted to proton elastic scattering. The relativistic wave functions provide goods fits to the p_m dependence of the data for quasiperpendicular kinematics even if the normalization factors for $Q^2 \geqslant 0.6$ (GeV/c)^2 are significantly larger than those for low Q^2. On the other hand, the normalization factors for the two Saclay experiments with quasiperpendicular kinematics do not agree well with each other either. Therefore, the failure of EMA-noSV calculations with NLSH wave functions to reproduce the p_m dependence of data for parallel kinematics with $T_p \lesssim 100$ MeV seems to be a more serious problem than the variation of normalization factors with Q^2. Recognizing that off-shell ambiguities are more serious for parallel kinematics because $x = Q^2/2m\omega$ varies over a wide range and expecting the reaction mechanism to be more reliable for large Q^2, we believe that the reaction mechanism for parallel kinematics with $T_p \lesssim 100$ MeV is not sufficiently reliable to justify fitting the bound-state wave function. Furthermore, it is likely that in such analyses, variations of the overlap function would tend to compensate for deficiencies in the reaction model.

If one wants to fit the momentum distribution for a discrete single-hole state to $(e,e'p)$ data, it is probably best to use quasifree kinematics where $(\omega, \boldsymbol{q})$ is constant and Q^2 is as large as possible. The reliability of the reaction mechanism should improve as Q^2 increases, and the use of quasifree kinematics should minimize distortion of $\rho(p_m)$ due to variation of the current operator off shell. It would then be of interest to test the reaction mechanism by comparison with data for parallel kinematics with large T_p. Ideally, such tests should have sufficient resolution in E_m to isolate discrete states without the complications of incoherent mixtures. Unfortunately, no high-resolution $(e,e'p)$ data for parallel kinematics with $T_p >$ 200 MeV and sufficient coverage in p_m are available.

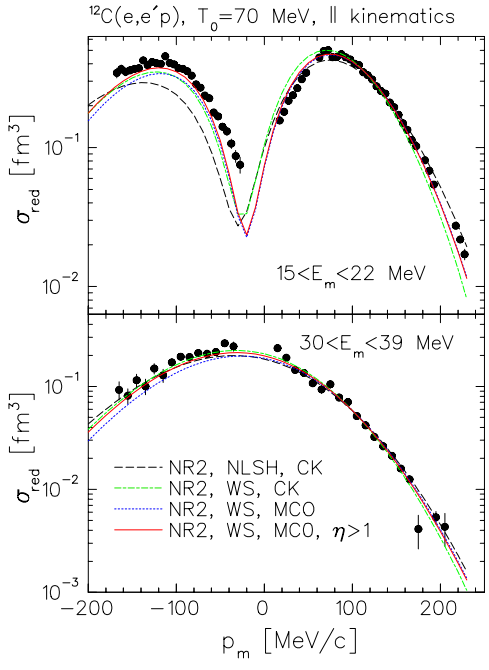

FIG. 9. (Color online) NR2 calculations for $^{12}C(e,e'p)$ compared with data from NIKHEF [18] using parallel kinematics for $T_p =$ 70 MeV/c. WS refers to the NIKHEF Woods-Saxon wave function, and $\eta > 1$ shows the effect of enhancing transverse components of the current operator.

V. RDWIA ANALYSIS

In this section, we analyze the data using full RDWIA calculations based upon Eq. (8) with Darwin nonlocality factors from Eq. (6) for NLSH and HS wave functions or Eq. (10) for NIKHEF wave functions.

A. Normalization factors

1. JLab

Full RDWIA fits to the JLab data [15] are shown in Fig. 10 using NLSH wave functions, EDAD1 optical potentials, and the CC2 current operator in Coulomb gauge. For the inclusive bin, these fits are slightly better than the corresponding EMA-noSV fits shown in Fig. 2 because full RDWIA calculations reproduce the left-right asymmetry better than the EMA-noSV approximation [14]. These fits for the $1p$ and $1s$ bins are significantly better than single-component fits because neither bin represents a pure single-particle configuration. The $1s$ contribution to the $1p$ bin fills in the minimum and rounds the peaks. Similarly, the $1p$ contribution to the $1s$ bin broadens the momentum distribution—the reduced $1s$ component provides a better fit for small p_m, while the $1p$ component improves the fit to larger p_m. However, for $p_m > 200$ MeV/c the data for both the s-shell and inclusive bins remain significantly above these two-component fits. Similar data for $^{16}O(e,e'p)$ [20,44] covering a broad range of missing energy show that for $p_m \gtrsim 150$ MeV/c there is much more strength at large E_m than can be attributed to single-nucleon knockout from the s shell. The continuum fraction increases with p_m, which may be simulated in the two-component model by a $1p$ admixture. Assuming that the $1s$ quasihole momentum distribution is similar to the Dirac-Hartree wave function, it would appear that the continuum contribution to $E_m > 30$ MeV has a broader momentum distribution than the $1p_{3/2}$ wave function used

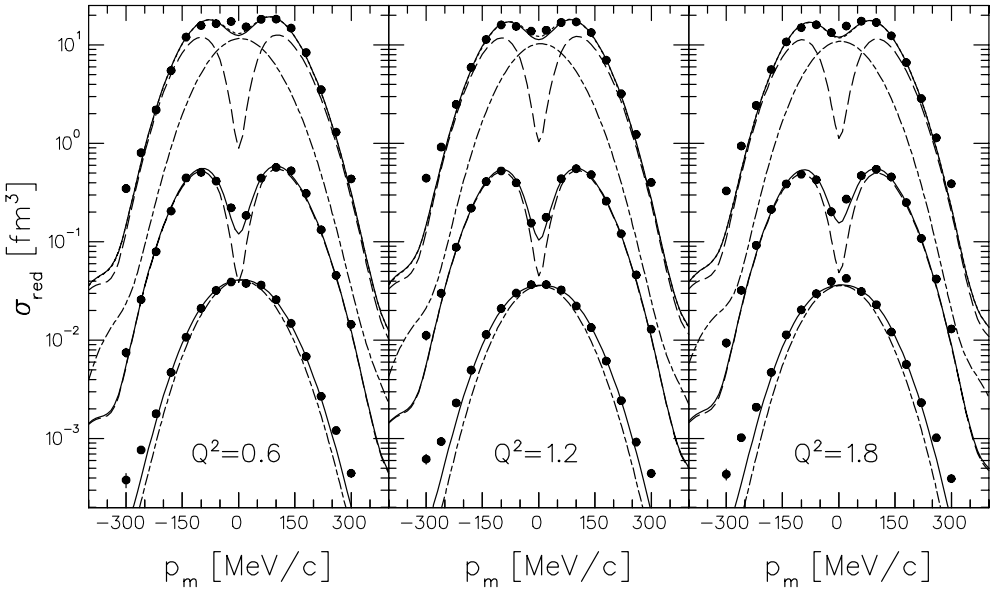

FIG. 10. Contributions of $1p_{3/2}$ and $1s_{1/2}$ fitted to JLab data for ^{12}C$(e, e'p)$. In each panel, the sets of curves show the same bins as in Fig. 2. The solid curves show the total fit; the dashed curves, the $1p$ contributions to the inclusive and p-shell bins; and the dash-dotted curves, the $1s$ contributions to the inclusive and s-shell bins. In addition, scale-factor fits for the IPSM are shown as dotted curves for the inclusive bin but are practically indistinguishable from the solid curves. All calculations use NLSH wave functions and EDAD1 optical potentials in full RDWIA.

in these two-component fits. Although part of this may be contributed by $1p$ fragmentation, much of the fitted $1p$ strength is probably a surrogate for multinucleon continuum. Recent SCGF estimates suggest that approximately 68% of the correlated continuum is in partial waves with $\ell \leqslant 1$ [45]. No doubt higher partial waves begin to contribute to the continuum as p_m increases, and it is likely that the $\ell = 1$ continuum is also broader than the $1p_{3/2}$ quasihole momentum distribution.

RDWIA fits to the JLab data using NLSH, HS, or NIKHEF wave functions are compared in Fig. 11. The two Dirac-Hartree wave functions provide very similar fits with a slight preference for NLSH. Mixing between $1p$ and $1s$ contributions improves fits to the $1s$ bin using NIKHEF wave functions by flattening the small p_m and lifting the large p_m regions. However, two-component fits using NIKHEF wave functions were impossible for the $1p$ bin because the $1s$ normalizations were negative; hence, the $1p$ NIKHEF fits

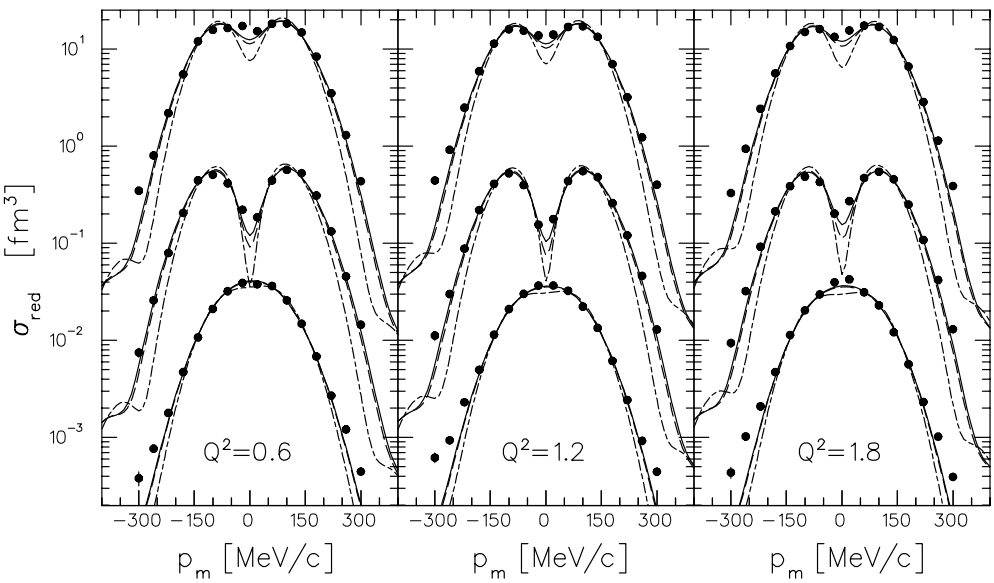

FIG. 11. RDWIA fits to the JLab data for JLab data for ^{12}C$(e, e'p)$ are compared for NLSH (solid), HS (dashed), and NIKHEF (dash-dot) wave functions. In each panel, the sets of curves show the same bins as in Figs. 2 and 10.

TABLE IV. Normalization factors for $^{12}C(e, e'p)$ fit to JLab data for three bins of missing energy and three values of Q^2 in $(GeV/c)^2$. The columns labeled *Ave* are averaged with respect to Q^2. The first set uses NLSH and the second HS wave functions. Both sets use EDAD1 optical potentials.

State	E_m (MeV) bin	NLSH				HS			
		$Q^2 = 0.6$	$Q^2 = 1.2$	$Q^2 = 1.8$	Ave	$Q^2 = 0.6$	$Q^2 = 1.2$	$Q^2 = 1.8$	Ave
$1p_{3/2}$	15–25	0.885	0.868	0.847	0.87	0.852	0.836	0.830	0.84
	30–50	0.060	0.078	0.077	0.072	0.063	0.058	0.062	0.061
	10–80	1.021	1.001	0.977	1.00	1.008	0.985	0.973	0.99
$1s_{1/2}$	15–25	0.133	0.102	0.198	0.14	0.082	0.050	0.110	0.08
	30–50	0.669	0.616	0.667	0.65	0.628	0.575	0.620	0.61
	10–80	0.953	0.887	1.009	0.95	0.818	0.757	0.845	0.81
IPSM	10–80	0.981	0.991	0.984	0.985	0.949	0.914	0.940	0.934

shown here simply scale RDWIA calculations for $1p_{3/2}$. Furthermore, the $1p$ NIKHEF fits are even worse, and their normalization factors are even smaller in RDWIA than in EMA-noSV: with EDAD1 those normalization factors are 0.66, 0.63, and 0.66 for RDWIA compared with 0.70, 0.67, and 0.69 for EMA-noSV at the three Q^2 settings. This reduction occurs because the RDWIA calculations for inherently nonrelativistic Woods-Saxon wave functions were made by replacing the Perey factor with the Darwin factor obtained using the spin-orbit potential, which leads to a narrower momentum distribution because the spin-orbit potential used by van der Steenhoven *et al*. [18] is stronger than that for NLSH or HS Dirac-Hartree wave functions. A narrower momentum distribution then requires a smaller normalization factor to reproduce the same peak cross section. The fits for the $1p$ bin overshoot the peaks and then fall too rapidly as p_m increases and these problems carry over, in slightly diluted form, to the inclusive bin. Therefore, we reject those parametrizations of the $1p_{3/2}$ and $1s_{1/2}$ overlap functions.

RDWIA normalization factors fitted to the JLab reduced cross section data for $^{12}C(e, e'p)$ in three bins of missing energy are collected in Table IV. These results were obtained using EDAD1 optical potentials, but the corresponding results for EDAD2, EDAD3, or EDAIC optical potentials differ by less than $\pm 5\%$ with systematics similar to Table II. Similar results were also obtained using more microscopic optical potentials based upon an empirical effective interaction (EEI) [46,47]. The differences between NLSH and HS results are small for $1p_{3/2}$ and modest for $1s_{1/2}$. Most of the discussion will be based upon the NLSH results because they provide slightly better fits to the data.

A rather large fraction, approximately 87%, of the IPSM $1p$ strength is found in the lowest E_m bin. If we assume that fragmentation of the $1p$ strength by collective modes is largely confined to excitation energies below 10 MeV, the 87% we find for the $1p$ shell is consistent with SCGF estimates. The additional $1p$ strength fitted to the reduced cross section for larger E_m probably represents continuum contributions with $\ell > 0$ that should not be added to the valence $1p$ strength.

The $1s$ contribution to the p-shell bin is more than predicted by Eqs. (17)–(18), but could arise either from resolution, discrete $\frac{1}{2}^+$ states, or a stronger low-E_m tail. Approximately 65% of the $1s$ IPSM strength appears in the $30 < E_m < 50$ MeV bin and corresponds to a net occupancy of 94% when scaled according to Eq. (19) to account for the spreading width. However, this is probably an overestimate of the $1s$ spectroscopic factor because one would expect approximately 10% of the $1s$ strength to lie beyond the 80 MeV missing energy; hence, if we scale N_{1s} for the NLSH fitted to the inclusive bin, we would obtain more than 100%. Although the overestimation appears to be smaller for the HS fits, neither accounts for continuum contributions from rescattering or two-body currents that could artificially enhance N_{1s}. The difficulties in reproducing the cross sections for $p_m > 200$ MeV/c in the $E_m > 30$ MeV region also suggest additional continuum contributions with broader momentum distribution that are not described by these two-component fits. Therefore, it is reasonable to assume that the depletion of the $1s$ shell by short-range correlations is similar to that for the $1p$ shell and to attribute the additional strength in the inclusive cross section to continuum processes that are not related directly to the single-hole spectral function.

The final line of Table IV lists IPSM scale factors fit to the $E_m < 80$ MeV data according to Eq. (16); these results are in reasonable agreement with the weighted average of the $1p$ and $1s$ normalization factors. The corresponding fits are shown in Fig. 10 as dotted curves that are practically indistinguishable from the two-component fits to the inclusive data. Therefore, we find approximately 98.5% of the IPSM strength in $E_m < 80$ MeV, which is considerably more than the 85% one expects after accounting for short-range correlations. It is likely that much of the extra strength observed for $E_m > 30$ MeV arises from processes other than single-nucleon knockout from the $1s$ shell, such that the total single-hole strength for $E_m < 80$ MeV is overestimated by this analysis.

Under these conditions, we consider $N_{1p}(15, 25) = 0.87$ to be the most reliable estimate of the depletion of IPSM orbitals in ^{12}C by short-range correlations. This estimate is consistent with the direct measurements of correlated continuum made by Rohe *et al*. [4] using parallel kinematics and the analysis of those data by Müther and Sick [45] based

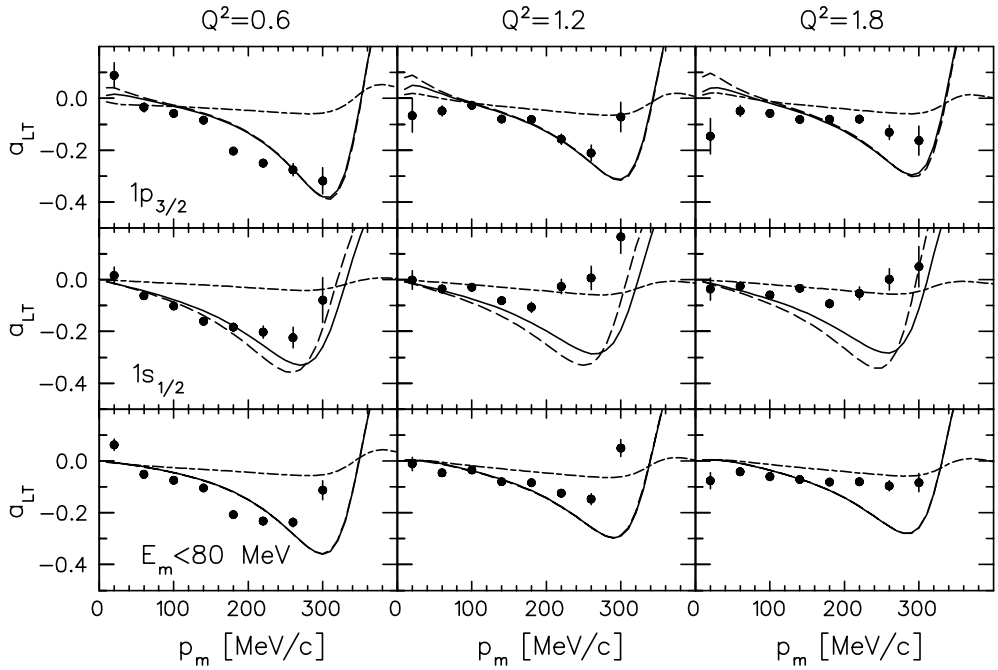

FIG. 12. RDWIA calculations for the left-right asymmetry in reduced cross section for quasiperpendicular kinematics with $0.6 \leqslant Q^2 \leqslant 1.8$ (GeV/c)^2. NLSH wave functions, EDAD1 optical potentials, and the CC2 current operator were used. Dashed curves show single-component calculations; solid curves, results for two-component $1p + 1s$ fits; dash-dotted curves, two-component fits in EMA-noSV.

upon SCGF. The extra yield observed by Dutta *et al.* [15] in quasiperpendicular kinematics should then be attributed to two-body currents and rescattering processes in which some of the flux absorbed by the optical potential is distributed to final states that remain within the experimental acceptance. Several studies suggest that rescattering contributions to the continuum are minimized for parallel kinematics [4,48,49]. These background contributions affect the interpretation of nuclear transparency measurements, which will be considered in Sec. V B.

For the sake of completeness, we also show in Fig. 12 the left-right asymmetry in reduced cross section

$$a_{\mathrm{LT}} = \frac{\sigma_{\mathrm{red}}(\phi = 0) - \sigma_{\mathrm{red}}(\phi = \pi)}{\sigma_{\mathrm{red}}(\phi = 0) + \sigma_{\mathrm{red}}(\phi = \pi)}, \tag{20}$$

where the azimuthal angle $\phi = 0$ corresponds to an ejectile momentum in the electron scattering plane between the beam direction and the momentum transfer. The sensitivity of this quantity to spinor distortion was studied in some detail in Ref. [14] for pure single-particle configurations. Figure 12 shows that the $1p_{3/2}$ admixture for the s-shell bin provides slightly better fits to the data for $p_m \lesssim 300$ MeV/c. That effect is small for the p-shell bin because the $1p$ admixture is small, and it is also small for the inclusive bin because the asymmetries for the two components are similar, depending more upon the Dirac potentials than upon the details of the bound-state wave functions. Two-component fits based upon EMA-noSV calculations demonstrate that $a_{\mathrm{LT}} \approx 0$ without spinor distortion because the characteristic left-right asymmetry for electron scattering by a moving free proton is removed by using the reduced cross section. The remaining asymmetry due to dynamical enhancement of lower components of Dirac spinors is described very well by RDWIA calculations. As argued in Ref. [14], the flattening of the p_m distribution for a_{LT} in the s shell and inclusive bins for increasing Q^2 is probably caused by continuum contributions that need not share the characteristic asymmetry of single-nucleon knockout.

2. Previous experiments

The RDWIA analysis of the JLab data presented in the preceding section provides a satisfying degree of internal consistency over a broad range of Q^2. Unfortunately, similar analyses for older data sets present a variety of consistency problems that cannot be resolved simply by choosing the best overlap functions or optical potentials. Therefore, in this section we consider those data in chronological order using only a single set of options, namely NLSH and EDAD1, in the RDWIA framework.

The fits shown in Fig. 13 appear to describe the Tokyo data [34] very well, but the $1s$ contribution to the p-shell bin is implausibly large. With NLSH wave functions and EDAD1 optical potential, we find $(N_{1p}, N_{1s}) = (0.56, 0.42)$ for $6 \leqslant E_m \leqslant 30$ MeV and $(N_{1p}, N_{1s}) = (0.08, 0.69)$ for $21 \leqslant E_m \leqslant 66$ MeV. Apparently there was an experimental problem in defining the p-shell or there is an unidentified problem in the reaction mechanism that enhances the cross section for small p_m. Because this is the only quasiperpendicular data set with severe problems in the p-shell bin for small

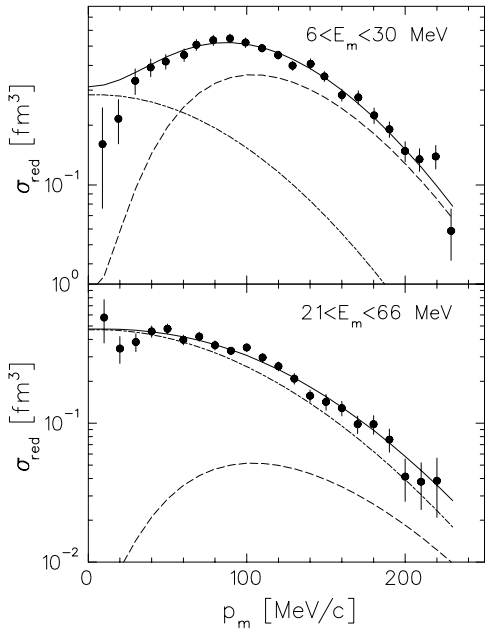

FIG. 13. RDWIA fit to Tokyo data [34] using NLSH wave functions. Solid curves show the fits; dashed and dash-dotted curves, $1p$ and $1s$ contributions.

p_m, we believe that energy resolution is a more likely explanation than reaction mechanism. The single-component fit to $p_m > 50$ MeV shown in Fig. 5 corresponds to $N_{1p} = 0.77$, which is more consistent with the other quasiperpendicular data for this bin. The $1p$ contribution to the $1s$ bin, on the other hand, is fairly small. Scaling the $1s$ fit for $21 \leqslant E_m \leqslant 66$ MeV according to Eq. (19) gives a net occupancy of 80%, which is reasonable but smaller than the corresponding JLab result. Perhaps the continuum contamination was smaller for the Tokyo experiment.

RDWIA provides no qualitative improvement over EMA-noSV fits to NIKHEF or Saclay data for parallel kinematics. As discussed before, we believe the severe variation of Bjorken x in parallel kinematics distorts momentum distributions fit to $(e, e'p)$ data for low Q^2 using familiar off-shell extrapolations of the single-nucleon current operator. Therefore, we do not consider those data further. Conversely, single-component RDWIA fits to the Saclay data for quasiperpendicular kinematics are similar to those shown in Figs. 3 and 4. There is no evidence for $1s$ contamination of the $15 \leqslant E_m \leqslant 25$ MeV bin, and the $30 \leqslant E_m \leqslant 50$ MeV bin is too narrow and the range of p_m is too small to find significant $1p$ strength there. Furthermore, mixed fits sometimes produce negative contamination factors with large uncertainties; hence, only single-component fits are considered for the Saclay quasiperpendicular data. We find $1p$ normalization factors of 0.63 for Ref. [35] or 0.75 for Ref. [32] that are somewhat smaller than the JLab results but are not in especially good agreement with each other either. Similarly, $N_{1s} = 0.46$ for 30–50 MeV corresponds to an occupancy of 67%, which is also somewhat less than the JLab result. Given that we believe the reaction mechanism is more reliable at higher Q^2 and that there are unresolved problems in reproducing data in parallel kinematics at the same Q^2, we are not especially alarmed by a 10–20% discrepancy between $Q^2 < 0.2$ and $Q^2 > 0.6$ (GeV/c)^2.

Finally, the statistical quality of the $1p$ SLAC data for $Q^2 = 1.1$ (GeV/c)^2 does not support extraction of a $1s$ admixture either. Nor did we attempt to fit the $1p$ contribution to the $30 \leqslant E_m \leqslant 80$ MeV bin because the enhancement for large positive p_m is probably an artifact of inadequate radiative unfolding. Single-component fits using RDWIA calculations are very similar to the EMA-noSV fits shown in Fig. 6, and the figures are omitted. The SLAC $1p$ normalization factor for the p-shell bin is 0.86 for NLSH and EDAD1, which is perfectly consistent with the JLab results. However, $N_{1s} = 1.2$ for 30–80 MeV is much larger than the JLab result and scaled up to unrestricted E_m would represent 140% of IPSM, suggesting a rather substantial underlying continuum.

3. Q^2 dependence of spectroscopic factors

Lapikás *et al.* [17] proposed that the Q^2 variation seen in their analysis of the spectroscopic factors for ^{12}C could be explained in terms of the resolution with which the electromagnetic knockout reaction probes the structure of a quasiparticle, such that the true spectroscopic factor would be observed in the limit $Q^2 \longrightarrow \infty$. Although this model was expressed in terms of a scale-dependent renormalization of the spectroscopic factor, it would be more appropriate to attribute such an effect, if present, to the single-nucleon current operator instead of to the spectroscopic factor. The overlap function for single-nucleon knockout takes the form

$$\left\langle \Psi_\alpha^{(A-1)} \middle| \Psi_0^{(A)} \right\rangle = \sum_\beta c_{\alpha\beta} \phi_\beta(\boldsymbol{r}), \tag{21}$$

where Ψ is a many-body state of either the A or $A-1$ nucleus, α is a state label with 0 being the target ground state, $c_{\alpha\beta}$ is a parentage coefficient, and ϕ_β is a local overlap function that is expected to resemble an orbital for the mean field. If the expansion basis is orthonormal, the spectroscopic factors become

$$S_\beta = \sum_\alpha |c_{\alpha\beta}|^2. \tag{22}$$

The parentage expansion depends upon the nuclear structure and is independent of the probe; hence, the spectroscopic factors should not depend upon Q^2. However, the assumption that the electromagnetic current operator is adequately approximated by the free nucleon current with the energy transfer placed on shell and with free form factors is questionable. Such approximations violate current conservation, Lorentz covariance, and unitarity. Furthermore, the current in a many-body system becomes nonlocal when expressed in terms of single-nucleon degrees of freedom; such nonlocality could contribute to an apparent scale dependence. Nevertheless, one must resort to simplified models of the current operator because there is no practical method for performing rigorous calculations for nucleon knockout from nuclei with $A > 2$. Therefore, Q^2 dependent modifications of the off-shell single-nucleon current operator should not be surprising.

The recent JLab data for ^{12}C show no evidence for systematic variations of the current operator within the range $0.6 \leqslant Q^2 \leqslant 1.8$ (GeV/c)^2. Although the consistency among previous experiments is not entirely satisfactory, our RDWIA analysis shows much less variation with Q^2 than suggested by Lapikás *et al*. Because the continuum contamination for $E_m > 30$ MeV has not been modeled accurately, we consider N_{1p} for the p-shell bin to be the most reliable gauge of possible Q^2 dependencies. Comparing the average of the two Saclay results for quasiperpendicular kinematics with the average of the JLab results for NLSH and EDAD1, we see an increase of $0.87/0.69 = 1.26$ compared with a factor of about 1.6 for $S_{1p} + S_{1s}$ from Ref. [17]. There may still be a small effect, which we would attribute to the current instead of to spectroscopic factors, but until the failure of RDWIA to reproduce low Q^2 data for parallel kinematics is understood, we are reluctant to interpret this as a simple scale factor.

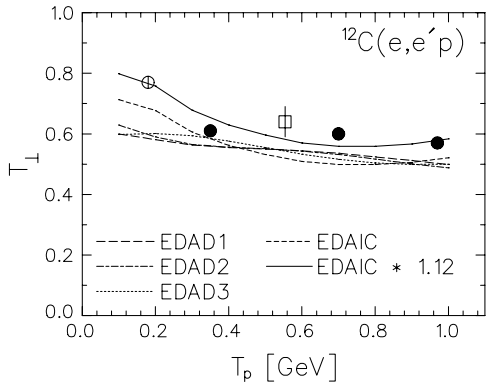

FIG. 14. RDWIA calculations using several optical potentials compared to transparency data for ^{12}C$(e, e'p)$. The solid curve has been multiplied by 1.12 to provide a better fit to the data from MIT (open circle), SLAC (open square), and JLab (filled circles). The SLAC datum includes systematic uncertainties, but other error bars are statistical only.

B. Transparency

The experimental definition of nuclear transparency

$$\mathcal{T}_{\rm exp} = \frac{\int_V d^3p_m dE_m d\Omega_e \sigma_{e,e'p}}{f \sum_\alpha \int_V d^3p_m dE_m d\Omega_e K \rho_\alpha(p_m) S_\alpha(E_m) \sigma_{ep}} \qquad (23)$$

compares the measured semi-inclusive differential cross section for proton knockout with a PWIA calculation based upon factorization of a model spectral function and the free e-p cross section. The phase-space volume is indicated by V, and we leave possible correction factors for nonuniform acceptance implicit, assuming that they are applied consistently in both numerator and denominator. Here K is a kinematic factor, $\rho_\alpha(p_m)$ is the momentum distribution for orbital α, $S_\alpha(E_m)$ is the energy distribution for single-nucleon removal from orbital α, and f is a correction factor describing the depletion of the single-hole spectral function by correlations that shift strength to large E_m. Dutta *et al*. [15] assumed that f is independent of α and obtained an estimate of 0.9 for ^{12}C from [36] that is consistent with the $1p$ normalization factor we extracted in the preceding section.

Similarly, a theoretical definition of nuclear transparency appropriate to quasiperpendicular kinematics takes the form

$$\mathcal{T}_\perp = \frac{\sum_\alpha \int dp_m\, p_m\, \sigma_{\rm RDWIA}(p_m, E_\alpha)}{\sum_\alpha \int dp_m\, p_m\, \sigma_{\rm RPWIA}(p_m, E_\alpha)} \qquad (24)$$

where the numerator integrates the RDWIA and the denominator the RPWIA cross section for the same model of the spectral function. For simplicity we neglect the spread of electron kinematics and assume quasifree kinematics for the ejectile, neglecting the small variation of transparency with nucleon kinetic energy within the acceptance. Similarly, we also neglect variations over the spreading widths of nuclear orbitals and assume that the bound-nucleon kinematics can be approximated by the IPSM. A more rigorous calculation would use Monte Carlo integration over a realistic model of the experimental acceptance, but the dependence of nuclear transparency upon energy is very mild and the differences between transparencies for parallel and quasiperpendicular kinematics are small [46].

Note that one should not include the correlation factor f in the theoretical definition of transparency because any strength that is removed from the numerator by correlations is also removed from the denominator by using the same spectral function for both. This factor is appropriate for Eq. (23) because the numerator integrates experimental yield while the denominator integrates a theoretical calculation based upon a model spectral function. When the denominator uses the IPSM, one requires a theoretical estimate for the fraction of the spectral strength that is shifted out of the experimental range of E_m. Unfortunately, a recent comparison of the data with RDWIA and Glauber calculations includes the correlation factor in both theoretical and experimental definitions of transparency [50], which we believe is incorrect.

RDWIA calculations using NLSH wave functions and several optical potentials from Dirac phenomenology [28] are compared in Fig. 14 with transparency data for ^{12}C$(e, e'p)$ from MIT [51], SLAC [36,52], and JLab [15,53]. The present results are very similar to those we previously obtained [46] using the EMA-noSV approximation and a definition of transparency that replaces the differential cross sections in Eqs. (23) and (24) with the corresponding reduced cross sections. Neither change is more than a couple percent. Our results are also similar to the RDWIA results of Lava *et al*. [50] after removal of the correlation factor. Also note that Lava *et al*. used a transparency definition based upon reduced cross section. However, Meucci [54] obtained somewhat larger transparency factors using an EMA-SV calculation based upon differential cross section. The latter are the only RDWIA calculations, of which we are aware, that overestimate the transparency for ^{12}C$(e, e'p)$, but the origin of their enhancement is not known.

The variation among A-independent global optical potentials is small, but the A-dependent potential fit to data for ^{12}C(p, p) provides the best description of the energy dependence for $T_p \lesssim 400$ MeV. However, all of these calculations

systematically underestimate the experimental transparency. Multiplying the EDAIC results by 1.12 provides a reasonable description of the data over this range of ejectile energy. Interestingly, this factor is very close to the inverse of the correlation correction applied by Abbott *et al.* [53]. If we assume that their correction factor is a reasonable estimate of the fraction of the single-nucleon yield shifted by correlations to large E_m, this comparison suggests that the experimental yield is approximately 12% larger than single-nucleon knockout. This is consistent with the fact that the RDWIA normalization factors sum to the full IPSM strength without depletion. Therefore, either the RDWIA is approximately 12% too absorptive or there is a significant continuum arising from multinucleon knockout that contributes approximately 12% of the strength for $E_m < 80$ MeV. The rather strong ^{16}O$(e, e'p)$ continuum seen in Fig. 21 of Ref. [20] suggests that the underlying continuum is probably responsible for the large normalization factors and transparency values for ^{12}C$(e, e'p)$.

The consistency between the fitted $1p$ normalization factors for $Q^2 > 0.6$ (GeV/c)^2 and the predicted IPSM depletion factor supports the accuracy of $(e, e'p)$ attenuation factors calculated using RDWIA with global optical potentials. The observation that the yield for $30 \leqslant E_m \leqslant 80$ MeV is considerably larger than can be attributed to $1s$ knockout demonstrates that there is significant background in the numerator that is not described by the spectral function used in the denominator of Eq. (23). The contribution to this background from multinucleon currents artificially increases the measured transparency insofar as that quantity is intended to represent the loss of flux from the single-nucleon knockout channel. However, the contribution to this background from rescattering processes that simply redistribute that flux within the experimental acceptance, instead of removing it entirely, represents a limitation of the distorted wave approximation which does not account for where flux "absorbed" by the optical potential finally appears [46]. The background fraction probably increases with A, but a more detailed model of the continuum is needed to distinguish between the processes that increase the experimental transparency with respect to RDWIA.

VI. SUMMARY AND CONCLUSIONS

We used RDWIA calculations based upon Dirac-Hartree bound-state wave functions to analyze data for ^{12}C$(e, e'p)$ for $E_m < 80$ MeV. Good fits are obtained for the recent JLab data [15] for $0.6 \leqslant Q^2 \leqslant 1.8$ (GeV/c)^2, with a slight preference for NLSH over HS wave functions and practically no variation with any of the optical potentials provided by Cooper *et al.* [28]. We find that the p-shell bin contains approximately 87% of the IPSM strength independent of Q^2 over that range. Although the s-shell bin appears to carry almost 100% of IPSM, independent of Q^2, there is evidence in the momentum distribution for a significant continuum that artificially increases the $1s$ normalization factor for two-component fits mixing $1p_{3/2}$ and $1s_{1/2}$ contributions. Therefore, we consider the $1p$ contribution to the $15 \leqslant E_m \leqslant 25$ MeV bin to be the most reliable estimate of the depletion of IPSM orbitals by short-range correlations; the occupancy of 87% is consistent with estimates based upon the self-consistent Green's function method and with recent direct measurements of the correlated continuum using parallel kinematics [4,45].

We also analyzed the same low Q^2 data sets used by Lapikás *et al.* [17] to study the Q^2 dependence of normalization factors for ^{12}C$(e, e'p)$. We found that the RDWIA calculations for Dirac-Hartree wave functions reproduce the low Q^2 data for quasiperpendicular kinematics well, but with somewhat smaller normalization factors. For example, the $1p$ normalization factors for two Saclay experiments were 0.63 and 0.75 using NLSH wave functions and EDAD1 optical potentials, compared with 0.87 for the JLab data. However, the same model fails to reproduce low Q^2 data for parallel kinematics, and remediation of this problem will require more than a multiplicative factor. Similar problems in previous NRDWIA analyses prompted van der Steenhoven *et al.* [18] to simultaneously adjust the Woods-Saxon wave function, the optical potential, and an empirical enhancement of the transverse components of the current. Although a better fit was achieved, this wave function does not reproduce the data for quasiperpendicular kinematics for either early low Q^2 experiments or the more recent high Q^2 experiments. The momentum distributions for the fitted Woods-Saxon wave functions are too narrow, which artificially reduces the normalization factors fit to data. Thus, Lapikás *et al.* [17] obtained a $1p$ normalization factor of only 0.56 for $Q^2 < 0.2$ (GeV/c)^2 and suggested that spectroscopic factors might depend strongly upon the resolution of the probe. We argue that spectroscopic factors are properties of nuclear structure that are independent of probe, but that the effective current operator for single-nucleon knockout may include additional Q^2 dependencies beyond those in familiar off-shell extrapolations of the free nucleon current operator. On the other hand, the additional Q^2 dependence is probably smaller than their estimate. Further investigation is needed to explain the discrepancy between parallel and quasiperpendicular kinematics at low Q^2—we believe that it is unwise to fit the momentum distribution to data with a strong variation of $x = Q^2/2m\omega$ in the absence of a more fundamental theory of the effective current operator.

Finally, we found that RDWIA calculations of nuclear transparency need to be multiplied by approximately 1.12 to reproduce data for ^{12}C and attribute much of this enhanced transparency to contributions to the continuum for $30 \leqslant E_m \leqslant 80$ MeV that are not directly related to single-nucleon knockout, such as multinucleon electromagnetic currents. However, a more detailed model of the continuum is need to distinguish between contributions due to multinucleon currents and those from rescattering processes.

ACKNOWLEDGMENTS

We thank Dr. Dutta for data tables and Dr. Udías for tables of the NLSH and HS wave functions. We especially thank Dr. Lapikás for the parameters of the NIKHEF wave functions and data tables for the Tokyo, Saclay, and SLAC experiments. The support of the U.S. National Science Foundation under Grant No. PHY-0140010 is gratefully acknowledged.

[1] L. Lapikás, Nucl. Phys. **A553**, 297c (1993).
[2] J. J. Kelly, Adv. Nucl. Phys. **23**, 75 (1996).
[3] S. Boffi, C. Giusti, F. D. Pacati, and M. Radici, *Electromagnetic Response of Atomic Nuclei* (Oxford University Press, Oxford, 1996).
[4] D. Rohe *et al*., Phys. Rev. Lett. **93**, 182501 (2004).
[5] T. Frick, K. S. A. Hassaneen, D. Rohe, and H. Müther, Phys. Rev. C **70**, 024309 (2004).
[6] W. H. Dickhoff and C. Barbieri, Prog. Part. Nucl. Phys. **52**, 377 (2004).
[7] O. Benhar, A. Fabrocini, and S. Fantoni, Phys. Rev. C **41**, R24 (1990).
[8] H. Müther and W. H. Dickhoff, Phys. Rev. C **49**, R17 (1994).
[9] H. Müther, A. Polls, and W. H. Dickhoff, Phys. Rev. C **51**, 3040 (1995).
[10] J. M. Udías, P. Sarriguren, E. Moya de Guerra, E. Garrido, and J. A. Caballero, Phys. Rev. C **51**, 3246 (1995).
[11] J. J. Kelly, Phys. Rev. C **60**, 044609 (1999).
[12] J. M. Udías, J. A. Caballero, E. Moya de Guerra, J. E. Amaro, and T. W. Donnelly, Phys. Rev. Lett. **83**, 5451 (1999).
[13] J. M. Udías and J. R. Vignote, Phys. Rev. C **62**, 034302 (2000).
[14] J. J. Kelly, arXiv:nucl-th/0501078 (unpublished).
[15] D. Dutta *et al*., Phys. Rev. C **68**, 064603 (2003).
[16] K. Garrow *et al*., Phys. Rev. C **66**, 044613 (2002).
[17] L. Lapikás, G. van der Steenhoven, L. Frankfurt, M. Strikman, and M. Zhalov, Phys. Rev. C **61**, 064325 (2000).
[18] G. van der Steenhoven, H. P. Blok, E. Jans, M. de Jong, L. Lapikás, E. N. M. Quint, and P. K. A. de Witt Huberts, Nucl. Phys. **A480**, 547 (1988).
[19] L. Frankfurt, M. Strikman, and M. Zhalov, Phys. Lett. **B503**, 73 (2001).
[20] K. G. Fissum *et al*., Phys. Rev. C **70**, 034606 (2004).
[21] C. J. Horowitz, D. P. Murdoch, and B. D. Serot, in *Computational Nuclear Physics I: Nuclear Structure*, edited by K. Langanke, J. A. Maruhn, and S. E. Koonin (Springer-Verlag, Berlin, 1991), pp. 129–151.
[22] L. G. Arnold, B. C. Clark, R. L. Mercer, and P. Schwandt, Phys. Rev. C **23**, 1949 (1981).
[23] Y. Jin and D. S. Onley, Phys. Rev. C **50**, 377 (1994).
[24] F. Perey and B. Buck, Nucl. Phys. **32**, 353 (1962).
[25] C. Giusti and F. D. Pacati, Nucl. Phys. **A473**, 717 (1987).
[26] T. de Forest, Nucl. Phys. **A392**, 232 (1983).
[27] P. Mergell, U.-G. Meissner, and D. Drechsel, Nucl. Phys. **A596**, 367 (1996).
[28] E. D. Cooper, S. Hama, B. C. Clark, and R. L. Mercer, Phys. Rev. C **47**, 297 (1993).
[29] C. J. Horowitz and B. D. Serot, Nucl. Phys. **A368**, 503 (1986).
[30] M. M. Sharma, M. A. Nagarajan, and P. Ring, Phys. Lett. **B312**, 377 (1993).
[31] L. Lapikás, private communication.
[32] M. Bernheim *et al*., Nucl. Phys. **A375**, 381 (1982).
[33] G. van der Steenhoven, H. P. Blok, E. Jans, L. Lapikás, E. N. M. Quint, and P. K. A. de Witt Huberts, Nucl. Phys. **A484**, 445 (1988).
[34] K. Nakamura and N. Izutsu, Nucl. Phys. **A259**, 301 (1976).
[35] J. Mougey, M. Bernheim, A. Bussière, A. Gillebert, P. X. Hô, M. Priou, D. Royer, I. Sick, and G. Wagner, Nucl. Phys. **A262**, 461 (1976).
[36] N. C. R. Makins *et al*., Phys. Rev. Lett. **72**, 1986 (1994).
[37] G. E. Brown and M. Rho, Nucl. Phys. **A372**, 397 (1981).
[38] J. Gao *et al*., Phys. Rev. Lett. **84**, 3265 (2000).
[39] K. I. Blomqvist *et al*., Phys. Lett. **B344**, 85 (1995).
[40] D. G. Ireland and G. van der Steenhoven, Phys. Rev. C **49**, 2182 (1994).
[41] K. W. McVoy and L. van Hove, Phys. Rev. **125**, 1034 (1962).
[42] J. R. Comfort and B. C. Karp, Phys. Rev. C **21**, 2162 (1980).
[43] J. J. Kelly, Phys. Rev. C **59**, 3256 (1999).
[44] N. Liyanage *et al*., Phys. Rev. Lett. **86**, 5670 (2001).
[45] H. Müther and I. Sick, Phys. Rev. C **70**, 041301(R) (2004).
[46] J. J. Kelly, Phys. Rev. C **54**, 2547 (1996).
[47] J. J. Kelly and S. J. Wallace, Phys. Rev. C **49**, 1315 (1994).
[48] I. Sick, in *Electron Nucleus Scattering*, edited by O. Benhar and A. Fabrocini (World Scientific, Singapore, 1997), p. 445.
[49] C. Barbieri and L. Lapikás, Phys. Rev. C **70**, 054612 (2004).
[50] P. Lava, M. C. Martínez, J. Ryckebusch, J. A. Caballero, and J. M. Udías, Phys. Lett. **B595**, 177 (2004).
[51] G. Garino *et al*., Phys. Rev. C **45**, 780 (1992).
[52] T. G. O'Neill *et al*., Phys. Lett. **B351**, 87 (1995).
[53] D. Abbott *et al*., Phys. Rev. Lett. **80**, 5072 (1998).
[54] A. Meucci, Phys. Rev. C **65**, 044601 (2002).